Computing and Informatics, Vol. 43, 2024, 317–342, doi: 10.31577/cai_2024_2_317

ADAPTIVE MATHEMATICAL MORPHOLOGY WITH FUZZY STRUCTURING ELEMENT

Mingzhu Zhang

College of Computer Science and Technology
Chongqing University of Posts and Telecommunications
Chongqing, China

Mengdi Sun

Dong'e Nanhu Xingzhi School
Liaocheng, China

Huichao Sun

School of Information Science and Engineering
Shandong Normal University
Jinan, China

Zhonggui Sun*

School of Mathematical Sciences
Liaocheng University
Liaocheng, China
e-mail: altlp@hotmail.com

Abstract. As a well-known nonlinear tool, mathematical morphology (MM) is still active in image processing. Benefiting from the fixed structuring element (SE),

* Corresponding author

traditional MM (TMM) gets solid theoretical foundation. However, due to the inherent diversity of pixels in an image, the rigid SE paradigm is not always practical. As a result, the development of morphology with adaptive SE, known as adaptive MM (AMM), has been a significant challenge. In this work, we present a novel approach for designing adaptive SE using the $\boldsymbol{\alpha}$-cut of a fuzzy set. By implementing dilation and erosion operations serially, we obtain an AMM (named SAMM) that is both adaptive to image content and robust to noise. Additionally, the operators in SAMM inherit important properties from TMM as much as possible. We provide theoretical proofs and simulated results to support our conclusion. Preliminary experiments on edge detection and noise reduction confirm the effectiveness of our SAMM both quantitatively and perceptually. In the denoising experiments, SAMM achieves the best performance in the nine algorithms involved, with its PSNR value surpassing the second-ranked approach by more than 0.6 dB overall. Additionally, its SSIM quantification metric also ranks prominently among the top performers.

Keywords: Adaptive morphology, fuzzy structuring element, serial implementation, stability

1 INTRODUCTION

Mathematical morphology (MM) was originally proposed for binary images [1, 2, 3, 4], and then developed to grey-level ones [5, 6, 7, 8]. Up to now, MM has been successfully applied in wide imaging applications, including edge detection [9, 10], image restoration [11], image segmentation [12, 13], and others [14, 15, 16, 17, 18]. Among the morphological operators, erosion and dilation are the two basic ones. Other operators, such as opening and closing, are generally formulated with the combinations of these two [19, 20]. The operators are all defined on a small component called structuring element (SE). With solid theoretical basis of lattices and topology [21, 22, 23], morphological operators usually have many important mathematical properties, including ordering, adjunction and idempotent [24, 25].

Traditional mathematical morphology (TMM) employs fixed-shaped structuring elements (SEs) for all pixels in an image, which may lead to undesired outputs. To address this issue, adaptive mathematical morphology (AMM) has been proposed, where the SE can adapt to the image content [26, 27]. Many AMMs have been developed [28, 29, 30, 31, 32, 33, 34, 35, 36, 37] with a focus on important mathematical properties and noise robustness [7, 24, 29, 38]. A comprehensive survey on this topic can be found in [27].

Recently, Graham Treece proposed a robust adaptive mathematical morphology (RAMM) that uses a rank strategy to make operators adaptive to content and robust to noise [39]. In this approach, the author directly plugs the operators from RAMM into a bitonic framework, resulting in a morphological filter [39] that reveals promising prospects and outperforms traditional filters such as NL-means [40] and

Guided filter [41], particularly in terms of visual results. However, as analyzed in subsection later, some crucial mathematical properties are missed for the operators from RAMM, making the theoretical basis of RAMM weaker than that of TMM. This motivates our work to address the shortcomings of RAMM.

Fuzzy sets extends the characteristic function from the binary values $\{0, 1\}$ to the unit interval $[0, 1]$ [42], providing a flexible tool for formulating problems and designing adaptive algorithms [43, 44]. Inspired by the fact, we employ a fuzzy SE to design our AMM. Compared with that in RAMM, the SE obtains two major advantages: symmetry and attention to the current pixel, as seen in classical filters like Gaussian and NL-means [40]. With the adaptive SE, serial implementations of the operators are designed, achieving a better trade-off between the adaptivity and robustness while preserving important properties.

Hereafter, we call our proposed AMM approach with serial operators SAMM. Figure 1 shows a denoising experiment on a one-dimensional signal, demonstrating the effectiveness of SAMM in noise removal and structure preservation.

The main contributions of this work are twofold:

- By defining the serial operators with fuzzy SE, we provide a novel mathematical morphology (SAMM), whose behaviors are not only adaptive to contents but also robust to noises.
- Theoretical proofs and numerical verifications both suggest that the operators in SAMM successfully inherit important mathematical properties from TMM, ensuring their reasonable behaviors in practice.

The remainder of this paper is organized as follows. Section 2 provides a brief review of related works, including TMM, RAMM and fuzzy set theory. In Section 3, we present the proposed SAMM and provide theoretical proofs for its mathematical properties. Section 4 evaluates SAMM through experiments. Finally, Section 5 concludes this paper.

2 KNOWLEDGE PREPARATION

Considering the closeness to this work, we briefly review related works, including TMM [20, 25], RAMM [39], and fuzzy set theory [42]. Additionally, we ntroduce the mathematical properties of the operators, such as ordering, adjunction, and idempotent. Furthermore, we define weak idempotent to describe the stability of the operators.

2.1 Traditional Mathematical Morphology

2.1.1 Definition

TMM considers a digital image f as a function from definition domain Ω to value field F. For a grey-level image with n pixels, Ω is a subset of Z^n, F is the set of grey

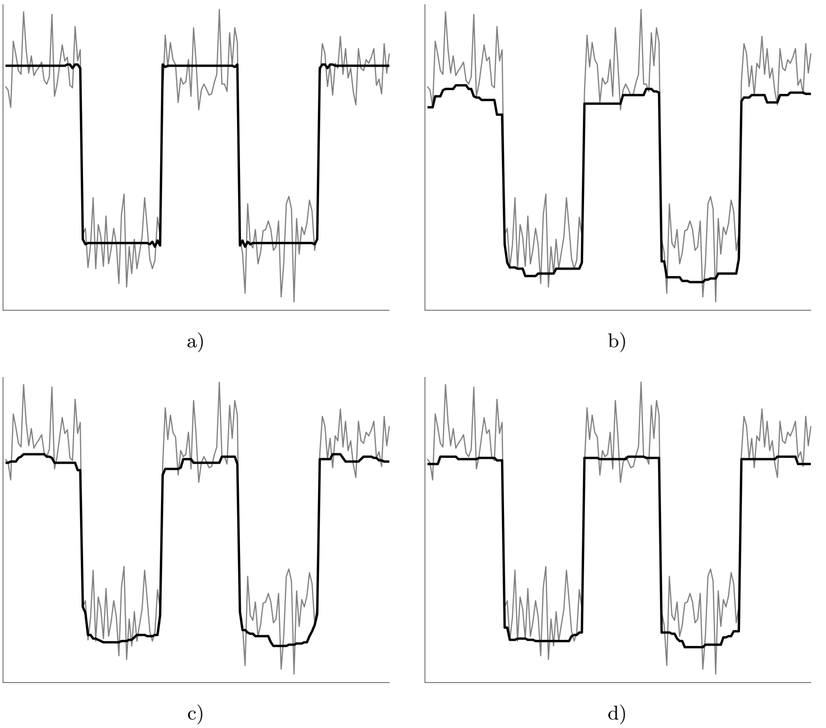

Figure 1. Comparison of the noise reduction on one-dimensional signal obtained by different morphological methods. To clearly show performance, the noisy input (grey curve) is embedded in every subfigure.

values. That is, the image f maps each pixel $x \in \Omega$ into $f(x) \in F$. Let $Fun(\Omega, F)$ denote the functions set from Ω to F, then $f \in Fun(\Omega, F)$ and $Fun(\Omega, F)$ compose a complete lattice [21, 22].

Morphological operators rely on a small component called Structuring Element (SE) which is used to probe and modify the image being studied. SEs can be classified into two categories based on their function values: flat and non-flat. A flat SE has constant or zero values at all coordinates, while a non-flat SE has various values. This means that flat SEs can avoid mixing spatial units with intensity values, and hence are applied more widely than non-flat ones in practice [20, 25]. In this paper, we also focus on flat SEs in designing mathematical morphology operators.

The two basic operators from MM, i.e., dilation (δ) and erosion (ε), are defined via maximizing and minimizing pixel values on a neighbourhood (determined by the structuring element, SE):

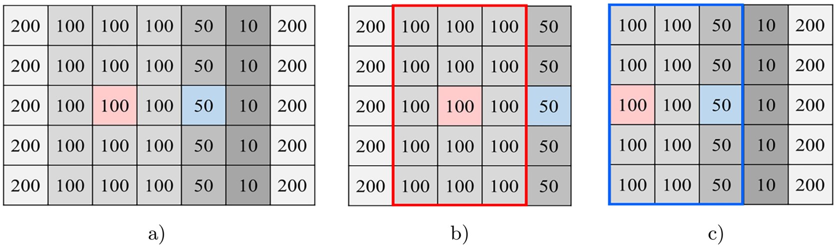

Figure 2. An instance of non-symmetric SE in RAMM. a) is an image region, two different pixels in which are marked in different colors. b) and c) respectively illustrate the adaptive SEs (in Equation (19), $c = 20$) of the two pixels in different color rectangles.

$$\delta_{SE}(f)(x) = \bigvee_{y \in SE} \{f(y)\}, \tag{1}$$

$$\varepsilon_{SE}(f)(x) = \bigwedge_{y \in \widehat{SE_x}} \{f(y)\}. \tag{2}$$

Here, SE_x is used to denote the definition domain of the SE with origin pixel x. $\widehat{SE_x}$ is the transposed SE (i.e., reflection w.r.t. the origin).

Go a step further, by combining the two basic operators, some other morphological operators such as opening (γ) and closing (ψ) can be defined:

$$\gamma_{SE}(f)(x) = \delta_{SE}\left(\varepsilon_{SE}(f)\right)(x), \tag{3}$$

$$\psi_{SE}(f)(x) = \varepsilon_{SE}\left(\delta_{SE}(f)\right)(x). \tag{4}$$

The definitions indicate that opening suppresses bright details smaller than the SE, while closing suppresses dark details. These operators are widely used in image processing tasks [19, 20].

2.1.2 Properties

As aforementioned, TMM is defined on a solid theoretical basis, which endows its operators with important properties that guarantee their reliable behavior.

One important property of TMM is the ordering relation between the two basic operators. For an image f, this property can be formulated as follows:

$$\varepsilon(f) \leq f \leq \delta(f). \tag{5}$$

With this property, the difference between dilation and erosion operations can be expressed as a non-negative value, which leads to the definition of the basic morphological gradient ρ (also called *Beucher gradient*):

$$\rho(f) = \delta(f) - \varepsilon(f). \tag{6}$$

200	200	200	200	200
200	200	200	200	200
200	200	**100**	200	200
200	200	200	200	200
200	200	200	200	200

a)

50	50	50	50	50
50	50	50	50	50
50	50	**100**	50	50
50	50	50	50	50
50	50	50	50	50

b)

Figure 3. An instance contradicting ordering property of the two basic operators from RAMM. a) and b) are two image regions, two current pixels with 100 grey value in them and are marked in different colors. For the SE settings in Equation (19), the threshold and the size of the rank filter window is 5×5. Under this condition, the dilation and erosion results of x and y are equal to 50 and 200, respectively.

Using the gradient, the boundaries or edges in the image can be detected [20, 24].

Another property introduced here is the adjunction, which comes from complete lattices and links the couple operators closely. For any two given images $f,\ g \in Fun(\Omega, F)$, (ε, δ) is an adjunction if and only if the following equation holds:

$$\delta\left(f\right) \leq g \Leftrightarrow f \leq \varepsilon\left(g\right). \tag{7}$$

Many works in designing morphologies strive to keep the adjunction relationship between the two basic operators [7, 24, 29]. With adjunction property, the idempotent of opening (closing) naturally holds, which can be described as

$$\left(\eta_{SE}\left(f\right)\right)^{n} = \eta_{SE}\left(f\right), \quad \forall n \geq 1, \tag{8}$$

where, f still represents an image, η denotes the opening γ (closing ψ). As pointed out in [45], idempotent indicates that the filter η has already affected the input as far as possible and hence further passes will not alter the signal any more. In this sense, idempotent reflects the stability of the filter's behavior.

However, as verified in the later section, idempotent is not always held in various MMs. To describe the stability of the operators conveniently, we define a weak idempotent as follows, which is a generalization of the traditional idempotent above.

Definition 1. For an operator η on image f, it is weak idempotent, if the following equation holds:

$$\exists k \in \mathrm{N} \Rightarrow \left(\eta_{SE}\left(f\right)\right)^{n} = \left(\eta_{SE}\left(f\right)\right)^{k}, \quad \forall n \geq k. \tag{9}$$

Here, the symbols represent the same meanings as those in Equation (8). Obviously, the smaller k means the more stability of the operator. Particularly, the weak

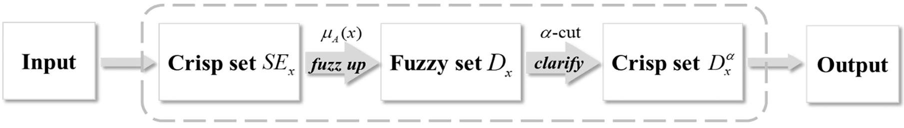

a)

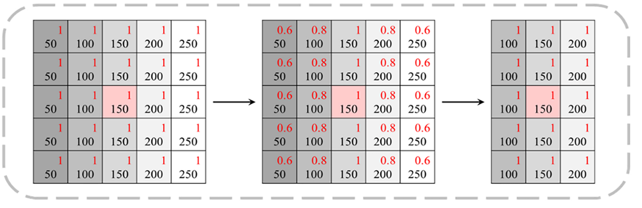

b)

Figure 4. The pipeline for SAMM. a) is the block diagram of the proposed method. b) is an instance to construct the SE in SAMM. The grey value of current pixel x is 150. The memberships of the fuzzy set D_x are marked in red, and the α-cut with threshold 0.8.

idempotent degenerates into the traditional one when $k = 1$, that is the most stable case.

2.2 Robust Adaptive Mathematical Morphology

Unlike many other adaptive methods being fragile to noises, RAMM [39] can be robust to noises. For a pixel x in image f, RAMM takes the rank filter of c^{th} centile as erosion:

$$r_{SE,c}(x) = c^{\text{th}} \underset{y \in SE_x}{centile}\{f(y)\}, \tag{10}$$

where SE_x still represents the SE centered at the current pixel x, which is also named filter window in [39]. c is recommended as a small centile.

Naturally, the dilation becomes

$$r_{SE,100-c}(x) = (100 - c)^{\text{th}} \underset{y \in SE_x}{centile}\{f(y)\}. \tag{11}$$

Go ahead, the closing and opening are respectively implemented as

$$C_{SE,c}(x) = r_{SE,c}\left(r_{SE,100-c}(x)\right), \tag{12}$$

$$O_{SE,c}(x) = r_{SE,100-c}\left(r_{SE,c}(x)\right). \tag{13}$$

Then, by plugging RAMM into a bitonic framework, the author presents an image filter as follows:

$$b_{SE,t}(x) = \frac{e_O(x) C_{SE,t}(x) + e_C(x) O_{SE,t}(x)}{e_O(x) + e_C(x)}, \tag{14}$$

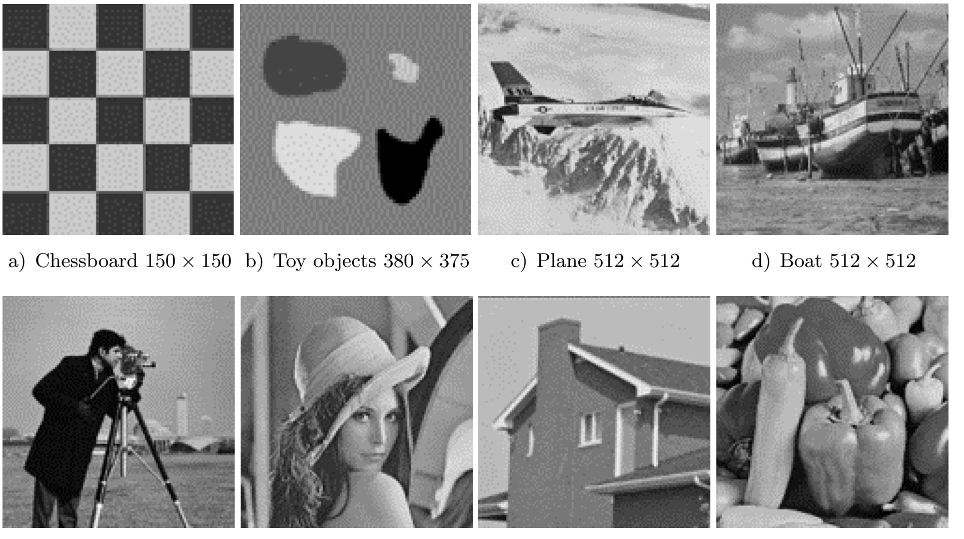

a) Chessboard 150×150 b) Toy objects 380×375 c) Plane 512×512 d) Boat 512×512

e) Cameraman 256×256 f) Lena 512×512 g) House 256×256 h) Peppers 512×512

Figure 5. Eight standard images that make up the test datasets for experiments

where $e_O(x)$ and $e_C(x)$ represent the difference between the original and opened/closed signals smoothed with Gaussian. For further details, see [39], where a filter defined in Equation (14) is presented that preserves edges and removes noise simultaneously, showing promising prospects.

However, as numerically validated later (Section 3.1), the operators in RAMM lack the important properties of ordering, adjunction, and idempotent that are present in TMM. This suggests that the theoretical foundation of RAMM is not as solid as TMM. In order to overcome this drawback, we propose a novel adaptive MM that ensures the operators have these important mathematical properties.

2.3 Fuzzy Sets

Since its inception half a century ago, the theory of fuzzy sets has found successful applications in various areas, such as image processing, pattern recognition, etc. [46, 47, 48]. A typical crisp set is originally defined with the characteristic function as follows:

$$\chi_X(x) = \begin{cases} 1, & x \in X, \\ 0, & x \notin X. \end{cases} \tag{15}$$

That is, as for the traditional set theory needs, the candidates must either belong to the set or not. In fuzzy set theory, the value set of the characteristic function is extend from $\{0, 1\}$ to $[0, 1]$, and then the function is recalled as membership function.

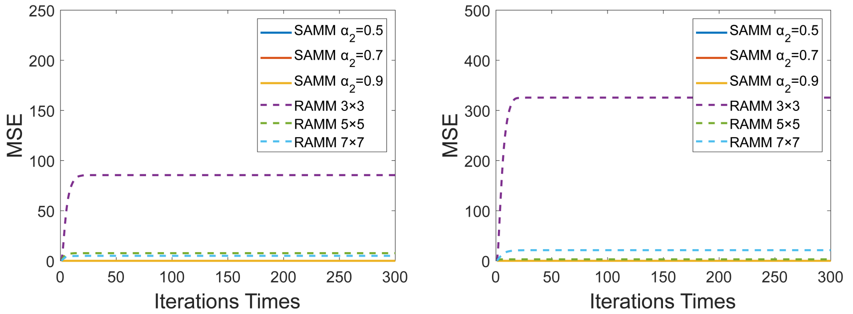

a) Fixed Opening

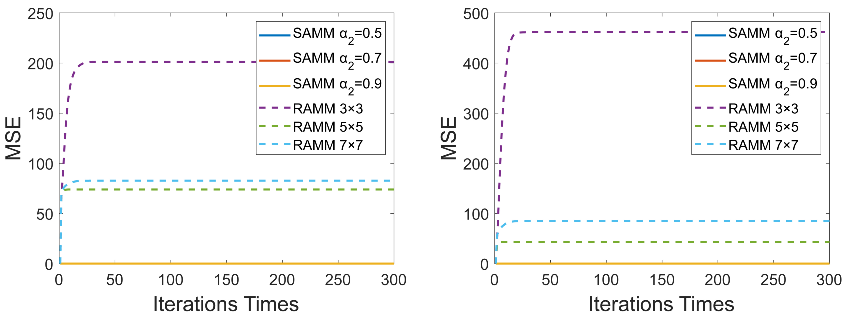

b) Fixed Closing

Let a classical set X denote definition domain, and the interval $[0,1]$ represent value field, the membership function of a fuzzy set A can be specified as

Property	Fixed Implementation	Dynamic Implementation
Symmetry of SE	$\surd$	$\surd$
Ordering	$\surd$	$\surd$
Adjunction	$\surd$	–
Idempotence	$\surd$	–

Table 1. Properties of the operators from SAMM

$$\mu_A(x) : X \to [0,1]. \tag{16}$$

Compared to classical sets, fuzzy sets allow for objects to have varying degrees of membership, resulting in a richer and more applicable value field.

In practice, a fuzzy set is inevitable to determine its members. To achieve the purpose, α-cut is introduced. Specifically, for every $\alpha \in [0,1]$, the α-cut of a given

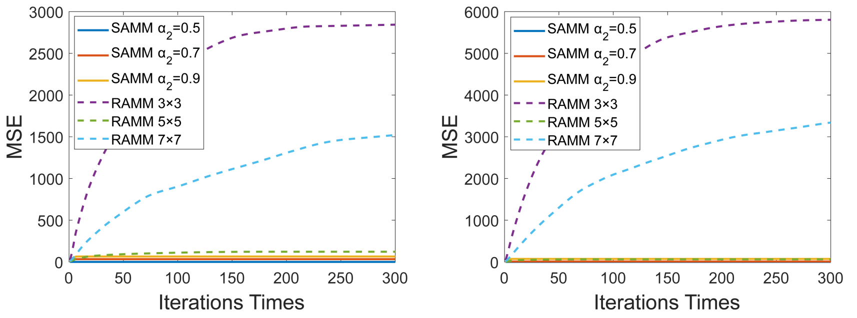

c) Dynamic Opening

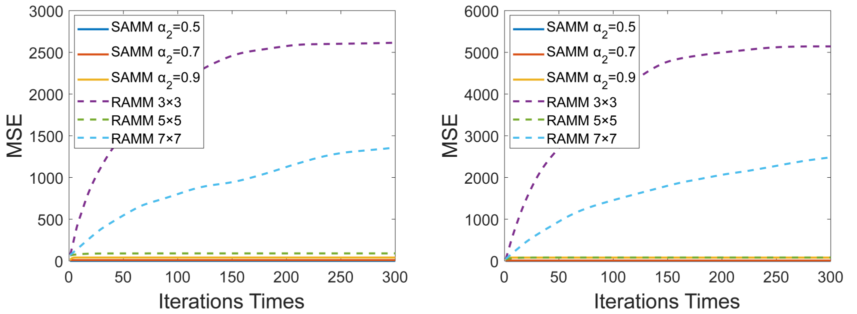

d) Dynamic Closing

Figure 6. Comparisons of stability between RAMM [25] and SAMM. MSE curves are computed between the n^{th} result and the first one on two images "House" (top row) and "Lena" (bottom row). a), b) report the opening and closing, respectively. They are both according to fixed implementation. c), d) describe the same operations according to dynamic implementation. The threshold α_2 is set to different values (0.5, 0.7, 0.9) in SAMM. Three SEs with different size (3×3, 5×5, 7×7) are employed in RAMM. The dotted lines and the solid ones represent the results of RAMM and SAMM, respectively.

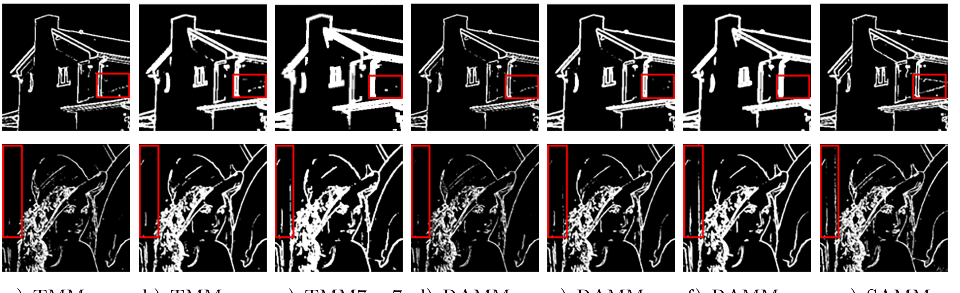

a) TMM 3×3 b) TMM 5×5 c) TMM7×7 d) RAMM 3×3 e) RAMM 5×5 f) RAMM 7×7 g) SAMM

Figure 7. Edge detection with *Beucher gradient* (defined in Equation (6))

Method	Fixed		Dynamic	
	Opening	Closing	Opening	Closing
RAMM 3×3	37	36	–	–
RAMM 5×5	11	9	119	108
RAMM 7×7	36	31	–	–
SAMM $\alpha_2 = 0.5$	1	1	1	1
SAMM $\alpha_2 = 0.7$	1	1	5	2
SAMM $\alpha_2 = 0.9$	1	1	8	9

Table 2. Minimum k in Definition 1 on "Lena"

fuzzy set A is defined as follows:

$$A^\alpha = \{x \in X \mid \mu_A(x) \geq \alpha\}. \tag{17}$$

Clearly, it is a crisp set derived from the fuzzy one. In this sense, α-cut is a bridge between fuzzy sets and crisp ones.

Method	Fixed		Dynamic	
	Opening	Closing	Opening	Closing
RAMM 3×3	31	32	–	–
RAMM 5×5	13	8	189	195
RAMM 7×7	30	29	–	–
SAMM $\alpha_2 = 0.5$	1	1	1	1
SAMM $\alpha_2 = 0.7$	1	1	2	3
SAMM $\alpha_2 = 0.9$	1	1	8	8

Table 3. Minimum k in Definition 1 on "House"

3 PROPOSED METHOD

With fuzzy SEs, we propose a novel adaptive morphology, SAMM, in this section. The serial implementation operators of SAMM are adaptive to image content, robust to noise, and possess important mathematical properties simultaneously. We first analyze the limitations of RAMM in Subsection 3.1, which provides the theoretical motivation for SAMM. Then, we provide a detailed design of SAMM in Subsection 3.2. The theoretical properties of the SAMM operators will be proven in Subsection 3.3.

3.1 Theoretical Motivation

To obtain the adjunction property of operators, the symmetry rule is generally pursued in designing adaptive SEs [7, 24, 29]. That is, for any $x, y \in \Omega$,

$$y \in SE_x \Leftrightarrow x \in SE_y. \tag{18}$$

Unfortunately, the SE in RAMM cannot satisfy this rule, and the basic operators in this morphology also fail to meet the ordering property. The detailed analysis is given below.

3.1.1 Non-Symmetry Analysis of RAMM

First, to reformulate RAMM in a typical method, an adaptive structuring element (SE) centered at pixel x is constructed as follows:

$$SE'_x = \{r_{SE,t}(x) \mid c \leq t \leq 100 - c\}. \tag{19}$$

Similar in Equation (10), c is still a threshold, $r_{SE,t}(x)$ is the output of rank filter defined on the window SE_x. Taking a step forward, we can reformulate the dilation and erosion of RAMM as follows:

$$\delta_{SE'}(f)(x) = \bigvee_{y \in SE'_x} \{f(y)\}, \tag{20}$$

$$\varepsilon_{SE'}(f)(x) = \bigwedge_{y \in SE'_x} \{f(y)\}. \tag{21}$$

Now, with maximization and minimization on SE'_x, the two basic operators originally defined in Equations (10) and (11) are now interpreted in typical ways.

Based on the aforementioned preparation, Figure 2 shows a simulated instance demonstrating that the SE defined in Equation (19) in RAMM is non-symmetric. In Figure 2 a), an image region is shown, with two pixels marked in red and blue, denoted by x and y, respectively.

The size of the rank filter window is set to 5×5, and the threshold $c = 20$. As a result, the adaptive SEs of the two pixels (i.e., SE'_x and SE'_y) are illustrated in Figures 2 b) and 2 c) in different rectangles. Clearly, $x \in SE'_y$ and $y \notin SE'_x$, that is contrary to the definition of symmetry in Equation (18). Therefore, the SE in RAMM does not meet symmetric property.

3.1.2 Non-Ordering Analysis of RAMM

Figure 3 illustrates that the ordering property is also no longer kept in the operators from RAMM. Here, Figures 3 a) and 3 b) are two image regions, the two pixels (x and y) in which are marked in red and blue, respectively. Using the same settings for SE as them in Figure 2, the dilation and erosion results of x and y are equal to 50 and 200, respectively. That means $\delta(f)(x) \leq f(x)$ and $\varepsilon(f)(y) \geq f(y)$, which contradicts the definition in Equation (5). Therefore, the ordering property cannot be met either in the two basic operators from RAMM.

3.2 Proposed Morphology (SAMM)

3.2.1 Construct Fuzzy SE

In TMM, the SE centered a pixel (i.e., SE_x) is a crisp set that leads to fix members. To get adaptivity, we first convert the crisp set to a fuzzy one with the following membership function:

$$\mu(y) = 1 - \frac{|f(y) - f(x)|}{255}, \quad (y \in SE_x)\,. \tag{22}$$

Here the membership $\mu(y)$ measures the similarity between the pixel y (in SE_x) and the current pixel x. Due to $\mu(x) = 1$, it pays great attention to x. Let D_x denote the fuzzy set constituted by the memberships, then

$$\mu(y) \in D_x \Leftrightarrow \mu(x) \in D_y. \tag{23}$$

That is, the fuzzy set is symmetric. Additionally, by assigning a threshold $\alpha \in [0, 1]$, the α-cut of D_x is achieved as

$$D_x^\alpha = \{y \in SE_x \mid \mu(y) \geq \alpha, x \in \Omega\}\,, \tag{24}$$

which is the SE in our SAMM. Bridging Equations (23) and (24), we know the SE is still symmetry. Meanwhile, it exhibits different robustness to noises according to different α. With an instance, Figure 4 presents the pipeline to construct SE in SAMM.

In a nutshell, compared with the structuring element $SE_x^{'}$ (in Equation (19)) in RAMM, the D_x^α designed above has two main advantages. On one hand, it is symmetric. On the other hand, like many classical filters, it pays more attention to the current pixel. As indicated later, the two changes make SAMM obtain important mathematical properties as much as possible.

3.2.2 Implement Operators Serially

When defining an adaptive morphology, the reflection of the SE is generally not recommended because it should be fully determined by the input contents [20, 25]. Therefore, we provide the embryonic forms of the two basic operators (i.e., dilation and erosion) as follows:

$$\delta_{D^\alpha}(f)(x) = \bigvee_{y \in D_x^\alpha} \{f(y)\}, \tag{25}$$

$$\varepsilon_{D^\alpha}(f)(x) = \bigwedge_{y \in D_x^\alpha} \{f(y)\}. \tag{26}$$

Here, the adaptability of the structuring element D_x^α enables the operators to exhibit adaptive behaviors. In particular, a larger α means less members belonging to the

SE, that is prone to protecting structures in the operations. Conversely, as α decreases, the operators become more robust to noises because of increasing members. To achieve a good balance between adaptivity and robustness, we adopt the serial forms [20] to implement the dilation and erosion in SAMM, as below:

$$\delta_{D^{\alpha_1}D^{\alpha_2}}(f)(x) = \delta_{D_x^{\alpha_1}}\left(\delta_{D_x^{\alpha_2}}(f)\right), \tag{27}$$

$$\varepsilon_{D^{\alpha_2}D^{\alpha_1}}(f)(x) = \varepsilon_{D_x^{\alpha_2}}\left(\varepsilon_{D_x^{\alpha_1}}(f)\right). \tag{28}$$

Here, $D_x^{\alpha_1}$ and $D_x^{\alpha_2}$ are two different SEs. For diversity, α_1 is usually recommended smaller than α_2.

3.3 Properties Discussion

To guarantee the operators possess important mathematical properties, for adaptive SEs, *"one has to fix the neighborhoods once they have been derived from an initial input image"* [7, 29]. That means, the SEs only rely on the initial input image, which is called fixed implementation. Otherwise, we call it dynamic implementation when the SEs are updated according to current inputs. Next, for the operators from the above two implementations of SAMM, we discuss their mathematical properties.

3.3.1 Fixed Implementation

For the fixed implementation of SAMM, we first focus on the two embryonic operators defined in Equations (25) and (26). Theorem 1 guarantees the ordering property, and Theorem 2 establishes the adjunction property. With Theorems 3 and 4, similar conclusions can be guaranteed for the serial forms adopted in SAMM, defined in Equations (27) and (28), respectively.

Theorem 1. For an image f of (Ω, F), and D_x^α is the SE centered at the current pixel x, a pair of operators (ε, δ) have the following ordering:

$$\varepsilon_{D^\alpha}(f) \le f \le \delta_{D^\alpha}(f), \quad \forall f \in Fun(\Omega, F).$$

Proof.

$$\begin{aligned}
&y \in D_x^\alpha, \quad \forall x \in \Omega \\
&\qquad \Rightarrow f(x) \in \{f(y)\}, \quad \forall x \in \Omega, y \in D_x^\alpha && \text{by (24)} \\
&\qquad \Rightarrow f(x) \le \bigvee_{y \in D_x^\alpha} \{f(y)\}, \quad \forall x \in \Omega \\
&\qquad \Rightarrow f(x) \le \delta_{D^\alpha}(f)(x), \quad \forall x \in \Omega && \text{by (25)} \\
&\qquad \Rightarrow f \le \delta_{D^\alpha}(f).
\end{aligned}$$

In a similar way, $f \ge \varepsilon_{D^\alpha}(f)$ can be deduced. Thus, $\varepsilon_{D^\alpha}(f) \le f \le \delta_{D^\alpha}(f)$. $\square$

Theorem 2. For any two given images f and g of (Ω, F), and D_x^α is the SE centered at the current pixel x, a pair of operators (ε, δ) is called an adjunction, if following equivalence holds:

$$\delta_{D^\alpha}(f) \leq g \Leftrightarrow f \leq \varepsilon_{D^\alpha}(g).$$

Proof.

$$\begin{aligned}
&\delta_{D^\alpha}(f) \leq g \\
&\qquad \Leftrightarrow \bigvee_{y \in D_x^\alpha} \{f(y)\} \leq g(x), \quad \forall x \in \Omega && \text{by } (25) \\
&\qquad \Leftrightarrow f(y) \leq g(x), \quad \forall x \in \Omega, \forall y \in D_x^\alpha \\
&\qquad \Leftrightarrow f(y) \leq g(x), \quad \forall y \in \Omega, \forall x \in D_y^\alpha && \text{by } (23) \\
&\qquad \Leftrightarrow f(y) \leq \bigwedge_{x \in D_y^\alpha} \{g(x)\}, \quad \forall y \in \Omega \\
&\qquad \Leftrightarrow f \leq \varepsilon_{D^\alpha}(g). && \text{by } (26)
\end{aligned}$$

□

Theorem 3. Suppose $(\delta_{D^{\alpha_1}}, \varepsilon_{D^{\alpha_1}})$ and $(\delta_{D^{\alpha_2}}, \varepsilon_{D^{\alpha_2}})$ are both ordering, then $(\varepsilon_{D^{\alpha_1}}\varepsilon_{D^{\alpha_2}}, \delta_{D^{\alpha_2}}\delta_{D^{\alpha_1}})$ is also ordering:

$$\varepsilon_{D^{a_1}}\varepsilon_{D^{a_2}}(f) \leq f \leq \delta_{D^{a_2}}\delta_{D^{a_1}}(f), \forall f \in Fun(\Omega, F).$$

Proof. Since $(\delta_{D^{\alpha_1}}, \varepsilon_{D^{\alpha_1}})$ and $(\delta_{D^{\alpha_2}}, \varepsilon_{D^{\alpha_2}})$ are both ordering, we get $\varepsilon_{D^{a_1}}(f) \leq f \leq \delta_{D^{a_1}}(f)$ and $\varepsilon_{D^{a_2}}(f) \leq f \leq \delta_{D^{a_2}}(f)$, by Theorem 1. Then

$$\begin{aligned}
&f \leq \delta_{D^{a1}}(f) \\
&\qquad \Rightarrow \delta_{D^{a2}}(f) \leq \delta_{D^{a1}}\left(\delta_{D^{a2}}(f)\right) \\
&\qquad \Rightarrow f \leq \delta_{D^{a2}}(f) \leq \delta_{D^{a1}}\left(\delta_{D^{a2}}(f)\right) \\
&\qquad \Rightarrow f \leq \delta_{D^{a1}}\left(\delta_{D^{a2}}(f)\right) \\
&\qquad \Rightarrow f \leq \delta_{D^{a1}}\delta_{D^{a2}}(f).
\end{aligned}$$

In a similar way, $f \geq \varepsilon_{D^{\alpha_1}}\varepsilon_{D^{\alpha_2}}(f)$ can be deduced. Thus, $\varepsilon_{D^{\alpha_1}}\varepsilon_{D^{\alpha_2}}(f) \leq f \leq \delta_{D^{\alpha_1}}\delta_{D^{\alpha_2}}(f)$. □

Theorem 4. Suppose $(\delta_{D^{\alpha_1}}, \varepsilon_{D^{\alpha_1}})$ and $(\delta_{D^{\alpha_2}}, \varepsilon_{D^{\alpha_2}})$ are both adjunction, then $(\varepsilon_{D^{\alpha_2}}\varepsilon_{D^{\alpha_1}}, \delta_{D^{\alpha_1}}\delta_{D^{\alpha_2}})$ is also adjunction:

$$\delta_{D^{a_1}}\delta_{D^{a_2}}(f) \leq g \Leftrightarrow f \leq \varepsilon_{D^{a_2}}\varepsilon_{D^{a_1}}(g), \forall f, g \in Fun(\Omega, F).$$

Proof. Since $(\delta_{D^{\alpha_1}}, \varepsilon_{D^{\alpha_1}})$ and $(\delta_{D^{\alpha_2}}, \varepsilon_{D^{\alpha_2}})$ are both adjunction, we get $\delta_{D^{a_1}}(f) \leq g \Leftrightarrow f \leq \varepsilon_{D^{a_1}}(g)$, $\delta_{D^{\alpha_2}}(f) \leq g \Leftrightarrow f \leq \varepsilon_{D^{\alpha_2}}(g)$ by Theorem 2. Then

$$\begin{aligned}
\delta_{D^{a1}}\delta_{D^{\alpha_2}}(f) \leq g & \\
&\Leftrightarrow \delta_{D^{a_1}}\left(\delta_{D^{a_2}}(f)\right) \leq g \\
&\Leftrightarrow \delta_{D^{\alpha_2}}(f) \leq \varepsilon_{D^{a_1}}(g) \\
&\Leftrightarrow f \leq \varepsilon_{D^{a_2}}\left(\varepsilon_{D^{a_1}}(g)\right) \\
&\Leftrightarrow f \leq \varepsilon_{D^{a_2}}\varepsilon_{D^{a_1}}(g).
\end{aligned}$$

$\square$

3.3.2 Dynamic Implementation

The difference between the fixed implementation and the dynamic one of SAMM only lies in the SEs being frozen or changed with the current (filtered) inputs. Thus, the SE still pays great attention to the current pixel in the dynamic implementation. Meanwhile, the proofs of Theorems 1 and 3 indicate that the operators of SAMM still meet ordering property. Moreover, Equations (22) and (24) tell us, the SEs employed in SAMM always keep symmetry regardless of the two implementations. However, as stated in [7], with changing SEs, the adjunction property cannot be satisfied. That means, the idempotent (defined in Equation (8)) of the operators from the dynamic implementation of SAMM cannot be guaranteed. For clarity, Table 1 summarizes the properties of the operators from the two different implementations of SAMM.

In a nutshell, compared with RAMM, our SAMM (regardless of the two different implementations) obtains more important mathematical properties.

Method	Time(s)	Overall means		Standard deviation σ									
				10		20		30		40		50	
		PSNR	SSIM	PSNR	SSIM	PSNR	SSIM	PSNR	SSIM	PSNR	SSIM	PSNR	SSIM
Input	–	20.10	0.306	28.18	0.601	22.21	0.353	18.81	0.244	16.51	0.184	14.78	0.146
TMM 3×3	0.32	27.04^{2}	0.676	30.78^{2}	0.850^{2}	28.56^{2}	0.764	26.72^{3}	0.669	25.22^{3}	0.585	23.91^{3}	0.514
TMM 5×5	0.32	26.08	0.724	28.85^{3}	0.815	27.23	0.773^{3}	25.93	0.724	24.77	0.675	23.61	0.632
TMM 7×7	0.31	24.74	0.719	27.25	0.783	25.87	0.753	24.73	0.718	23.62	0.687	22.25	0.652
RAMM 3×3	3.56	23.28	0.681	26.62	0.829^{3}	24.89	0.761	23.11	0.679	21.57	0.601	20.21	0.534
RAMM 5×5	3.35	26.40^{3}	0.758^{2}	28.23	0.818	27.28^{3}	0.792^{2}	26.34^{2}	0.761^{2}	25.47^{2}	**0.726^{1}**	24.67^{2}	0.691^{2}
RAMM 7×7	3.49	24.61	0.742^{3}	25.65	0.778	25.23	0.762	24.65	0.744^{3}	24.05	0.723^{2}	23.45	**0.703^{1}**
NLMM [7] 7×7	3771	21.84	0.612	28.16	0.665	23.92	0.637	21.10	0.622	18.81	0.601	17.85	0.533
NLMM [24] 7×7	3771	21.72	0.582	25.90	0.573	22.57	0.501	21.01	0.560	20.10	0.645	19.04	0.630
SAMM	6.49	**27.87^{1}**	**0.767^{1}**	**31.23^{1}**	**0.855^{1}**	**29.20^{1}**	**0.812^{1}**	**27.58^{1}**	**0.768^{1}**	**26.28^{1}**	0.722^{3}	**25.05^{1}**	0.678^{3}

Table 4. Average values of PSNR (dB) and SSIM on 8 images using OCCO framework. The best three results are indicated by their ranking, with ^{1} also in bold

Method	Time(s)	Overall means		Standard deviation σ									
				10		20		30		40		50	
		PSNR	SSIM	PSNR	SSIM	PSNR	SSIM	PSNR	SSIM	PSNR	SSIM	PSNR	SSIM
Input	–	20.10	0.306	28.17	0.601	22.21	0.353	18.82	0.244	16.50	0.184	14.78	0.146
TMM 3×3	0.36	26.86	0.585	32.83^{2}	0.847	28.77	0.683	26.07	0.550	24.09	0.456	22.55	0.389
TMM 5×5	0.35	27.90	0.690	32.39^{3}	0.863^{3}	29.45^{3}	0.767	27.35	0.674	25.81	0.601	24.50	0.544
TMM 7×7	0.38	28.03^{2}	0.729	31.90	0.860	29.39	0.790	27.61^{3}	0.721	26.23	0.663	25.02^{3}	0.613
RAMM 3×3	2.36	26.59	0.612	30.79	0.844	28.45	0.714	26.28	0.591	24.48	0.494	22.93	0.419
RAMM 5×5	2.36	28.01^{3}	0.736^{2}	31.48	0.867^{2}	29.47^{2}	0.805^{3}	27.76^{2}	0.734^{2}	**26.29^{1}**	0.666^{2}	25.03^{2}	0.607^{3}
RAMM 7×7	2.27	27.43	**0.759^{1}**	29.75	0.852	28.60	**0.811^{1}**	27.39	**0.761^{1}**	26.24^{3}	**0.709^{1}**	**25.18^{1}**	**0.660^{1}**
NLMM [7] 7×7	2 067	23.31	0.634	29.26	0.722	24.05	0.645	23.40	0.600	20.85	0.625	18.99	0.579
NLMM [24] 7×7	2 072	22.81	0.618	26.76	0.607	23.09	0.581	24.05	0.677	21.08	0.645	20.40	0.580
SAMM	4.18	**28.64^{1}**	0.738^{2}	**33.63^{1}**	**0.879^{1}**	**30.38^{1}**	0.806^{2}	**28.12^{1}**	0.732^{3}	26.28^{2}	0.664^{3}	24.77	0.608^{2}

Table 5. Average values of PSNR (dB) and SSIM on 8 images using bitonic framework. The best three results are indicated by their ranking, with ^{1} also in bold.

4 EXPERIMENTS

The experiments in this section evaluate the stability and performance of RAMM and SAMM, using both fixed and dynamic implementations. The edge detection and noise reduction experiments focus only on dynamic methods to achieve optimal results. This work mainly focuses on designing an adaptive mathematical morphology (SAMM), whose operators can inherent important properties from traditional mathematical morphology (TMM) as much as possible. Considering this motivation, the filters involved in our experiments for edge detection and image denoising are all from mathematical morphologies.

For SAMM, we naively fix α_1 with 0 and only set α_2 empirically in the SEs $D_x^{\alpha_1}$ and $D_x^{\alpha_2}$. Considering unwanted structures that cannot be removed with a small SE and useful structures that may be damaged with a large SE, we set the window size of the two SEs 3×3 and 5×5, respectively.

Besides TMM and RAMM, two other adaptive morphological morphologies, i.e., non-local mathematical morphologies (NLMM), are also involved in the denoising experiments, which were proposed in [7] and [24], respectively. For TMM and RAMM, three different sizes (3×3, 5×5, 7×7) of SEs are separately used to search the ideal results. Other parameters of RAMM and the two NLMMs all follow the original settings.

As shown in Figure 5, we conducted experiments on eight standard images, including two cartoon images and six natural ones. To handle the neighborhood outside the image areas, we used a symmetrical padding strategy as the SEs were slid over the input images.

4.1 Stability Test

With different (fixed and dynamic) implementations of SAMM and RAMM, the opening and closing are both iterated 300 times on "House" and "Lena". To be objective, the α_2 in SAMM is assigned to different values (0.5, 0.7 and 0.9).

Tables 2 and 3 list the minimum k in the weak idempotent (Definition 1, subsection 3.1.2)) on the two images, respectively. As aforementioned, the smaller k means the more stable performances, and $k = 1$ corresponds to the typical idempotent. Clearly, the operators from fixed implementation of SAMM all meet idempotent, which is consistent with Theorem 4. Meanwhile, for dynamic implementation, the k are all not greater than 10. That means, the operators from SAMM all become stable within 10 iterations. On the other side, for RAMM, even for the most stable case (with 5×5 SE in the fixed implementation), it still cannot meet idempotent ($k > 1$).

For RAMM, as analyzed in Subsection 3.1, despite its meaningful performance, its SEs are not symmetric and the ordering property of the operators no longer hold. Additionally, due to the significance of symmetry property in proving Theorem 2, the adjunction property of the operators from RAMM cannot be guaranteed theoretically. That means, the idempotent cannot be guaranteed either.

For dynamic implementation of RAMM, the k are all greater than 100 disastrously. The curves of mean square error (MSE) between the n^{th} opening (closing) result and the first one plotted in Figure 6 also agree with the quantitative results from Tables 2 and 3. In summary, compared to RAMM, SAMM exhibits more stable behaviors.

Note that, as stated in [39], *"It must be acknowledged that PSNR and SSIM are not complete measures of image quality, and are not responsive to small but visually distracting artefacts."* Therefore, visual results for the two frameworks are presented in Figures 8 and 9, in addition to the quantitative indicators. The figures include magnified fragments of the noisy inputs ($\sigma = 20$) and the denoised results for comparison.

As shown there, although TMM can preserve image details well using small (3×3) SEs, it cannot effectively remove the noises. Additionally, many patchy artifacts arise due to the low-level ability of smoothing. With large (7×7) SEs, the images are over-smoothed, causing noticeable geometrical structures to be damaged. Due to the rigidity of shape and size, using 5×5 SEs, TMM cannot get a satisfying trade-off either. With the help of adaptivity and robustness advantages, RAMM gets better results. Particularly, with 5×5 SEs, the operators from RAMM achieve a nice balance between denoising and structure-preserving.

4.2 Edge Detection

We conducted an edge detection experiment on two standard images using SAMM, TMM, and RAMM, where the *Beucher gradient* (defined in Equation (6)) is used to describe edges. The parameters of TMM and RAMM are kept the same as in the beginning of the section, while the parameter in SAMM is set to 0.95 empirically.

The frozen shape and fixed size of SEs in TMM oversmooth several small structures in the outputs, while RAMM achieves better edge preservation due to its adaptivity. However, RAMM's operators fail to meet the ordering property, which

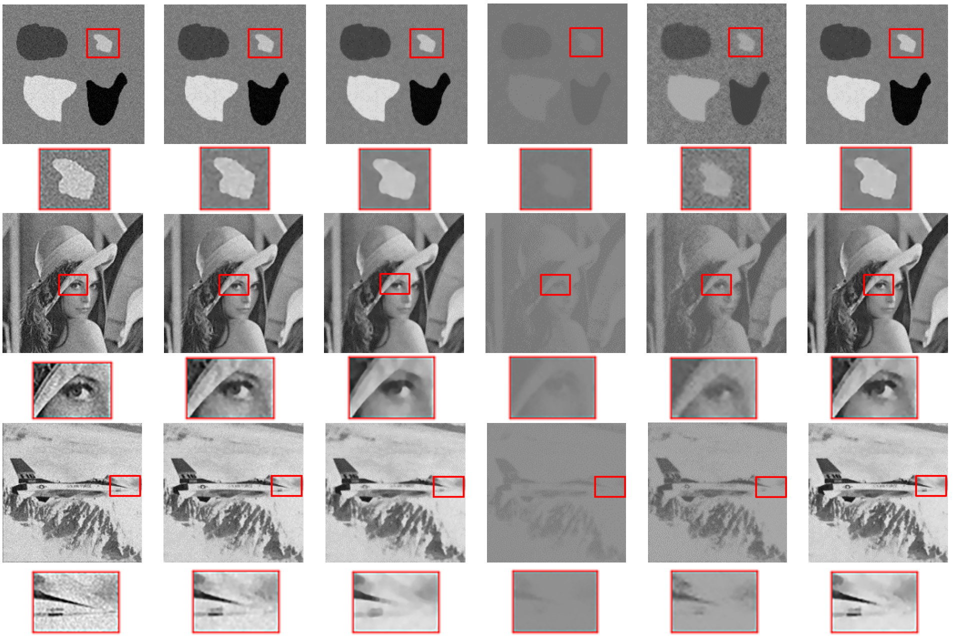

Figure 8. Noise reduction using OCCO framework. The local magnifications are also presented in red rectangles.

affects its performance. In contrast, the operators from SAMM, which possess mathematical properties such as symmetry and ordering, exhibit the best performance among the competitors. The results are validated with the regions marked by the red rectangles in Figure 7.

4.3 Noise Reduction

To evaluate their denoising performance, we apply the morphological operators to two methods: the opening-closing and closing-opening (OCCO) [49] and the bitonic filter, which is a weighted average of opening and closing originally proposed in [39] and reformulated in Equation (14) for convenience. We conduct the experiment on the image set (shown in Figure 5) by adding white Gaussian noise with different standard deviations ($\sigma = 10, 20, 30, 40, 50$). Following the parameter settings at the beginning of this section, we only modify the parameter α_2 in SAMM for different tasks. Here, the linear model is employed to describe the relationship between this parameter and the standard deviation. Specifically, $\alpha_2 = 1 - 0.002 \cdot \sigma$ for the OCCO framework and $\alpha_2 = 1 - 0.005 \cdot \sigma$ for the bitonic framework.

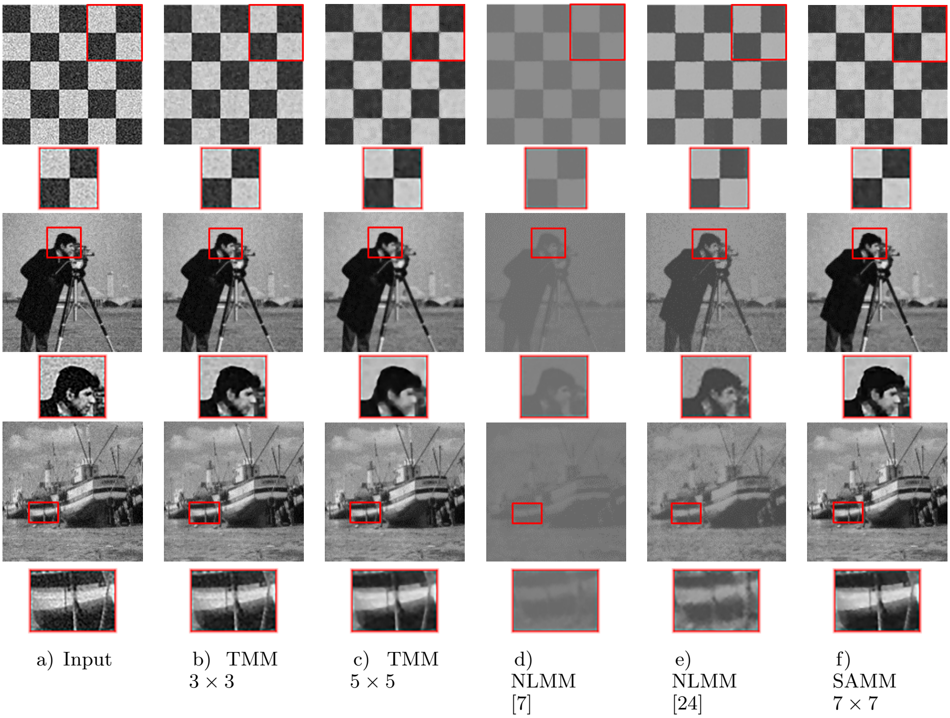

Figure 9. Noise reduction using bitonic framework. The local magnifications are also presented in red rectangles.

Two typical indicators, i.e., peak signal to noise ratio (PSNR) and structural similarity (SSIM) [50], are both used to make the comparison. Table 4 and Table 5 respectively report the quantitative results in the two denoising frameworks, where the average indicator values on the eight images are listed. On one hand, as indicated in Table 4, in the OCCO framework, SAMM always obtains the best PSNR. Meanwhile, according to SSIM, our SAMM also almost outperforms its all rivals. On the other hand, Table 5 demonstrates that the bitonic framework improves the performance of most of the denoisers to various extents, with SAMM still exhibiting powerful performance. Simultaneously, the run time of the counterparts are all reported. We can see that, SAMM runs twice as long as RAMM due to its serial implementations.

5 CONCLUSION

In adaptive morphology studies, maintaining important mathematical properties of operators has always been pursued by experts. However, achieving a satisfactory balance between these properties and performance is a challenging task. To address this issue, we propose an adaptive mathematical morphology (SAMM) using fuzzy set theory to define serial operators. SAMM operators inherit key mathematical properties from traditional morphological operators while exhibiting both adaptivity and robustness. Mathematical proofs and simulations confirm these advantages. Preliminary experiments on edge detection and noise reduction confirm the effectiveness of our proposed methodology both quantitatively and perceptually. Among the nine algorithms tested in the denoising experiments, SAMM stands out as the top performer, achieving a PSNR value that surpasses the second-ranked approach by more than 0.6 dB overall.

It should be noted that although we have provided a preliminary analysis of the stability of SAMM in dynamic implementation and have numerically verified its weak idempotence, further investigation is needed to guarantee its stability with rigorous theories. Additionally, we would like to point out that the morphological neural network (MNN), which combines mathematical morphology with deep neural networks, has recently emerged as a promising tool [51, 52, 53]. Therefore, how to incorporate adaptive morphology into MNN is also worthy of further studying.

Acknowledgement

This work was supported in part by the National Natural Science Foundation of China under Grant No. 11801249, the Nature Science Foundation of Shandong Province China under Grant No. ZR2020MF040, and in part by the Open Project of Liaocheng University under Grant No. 319462207-1.

REFERENCES

[1] Charif-Chefchaouni, M.—Schonfeld, D.: On the Invertibility of the Morphological Representation of Binary Images. IEEE Transactions on Image Processing, Vol. 3, 1994, No. 6, pp. 847–849, doi: 10.1109/83.336253.

[2] Jin, X. C.—Ong, S. H.—Jayasooriah: A Domain Operator for Binary Morphological Processing. IEEE Transactions on Image Processing, Vol. 4, 1995, No. 7, pp. 1042–1046, doi: 10.1109/83.392348.

[3] Nadadur, D.—Haralick, R. M.: Recursive Binary Dilation and Erosion Using Digital Line Structuring Elements in Arbitrary Orientations. IEEE Transactions on Image Processing, Vol. 9, 2000, No. 5, pp. 749–759, doi: 10.1109/83.841511.

[4] Hedberg, H.—Dokladal, P.—Owall, V.: Binary Morphology with Spatially Variant Structuring Elements: Algorithm and Architecture. IEEE Transactions on Image Processing, Vol. 18, 2009, No. 3, pp. 562–572, doi: 10.1109/TIP.2008.2010108.

[5] Heijmans, H. J. A. M.: Theoretical Aspects of Gray-Level Morphology. IEEE Transactions on Pattern Analysis and Machine Intelligence, Vol. 13, 1991, No. 6, pp. 568–582, doi: 10.1109/34.87343.

[6] Bouaynaya, N.—Charif-Chefchaouni, M.—Schonfeld, D.: Theoretical Foundations of Spatially-Variant Mathematical Morphology Part I: Binary Images.

IEEE Transactions on Pattern Analysis and Machine Intelligence, Vol. 30, 2008, No. 5, pp. 823–836, doi: 10.1109/TPAMI.2007.70754.

[7] Velasco-Forero, S.—Angulo, J.: On Nonlocal Mathematical Morphology. In: Hendriks, C. L. L., Borgefors, G., Strand, R. (Eds.): Mathematical Morphology and Its Applications to Signal and Image Processing (ISMM 2013). Springer, Berlin, Heidelberg, Lecture Notes in Computer Science, Vol. 7883, 2013, pp. 219–230, doi: 10.1007/978-3-642-38294-9_19.

[8] Hÿtch, M.—Hawkes, P. W.: Morphological Image Operators. Academic Press, 2020.

[9] Sun, X.—Wang, X. Y.—Luo, Z. R.—Xiao, H.: Research on the Edge Detection Algorithm of Smokescreen Based on Mathematical Morphology. Applied Mechanics and Materials, Vol. 610, 2014, pp. 429–436, doi: 10.4028/www.scientific.net/AMM.610.429.

[10] Shui, P. L.—Wang, F. P.: Anti-Impulse-Noise Edge Detection via Anisotropic Morphological Directional Derivatives. IEEE Transactions on Image Processing, Vol. 26, 2017, No. 10, pp. 4962–4977, doi: 10.1109/TIP.2017.2726190.

[11] Jiang, L. H.—Jin, Z. N.—Zhang, F.—Liu, R. H.: A New Algorithm for Speckle Suppression Using Mathematical Morphology and Adaptive Weighted Technique. 2007 International Conference on Machine Learning and Cybernetics, Vol. 5, 2007, pp. 2427–2430, doi: 10.1109/ICMLC.2007.4370553.

[12] Lee, H. G.—Lee, S. C.: Morphological Multi-Cell Discrimination for Robust Cell Segmentation. IEEE Access, Vol. 8, 2020, pp. 49837–49847, doi: 10.1109/ACCESS.2020.2980561.

[13] Zhang, Q.—Zhou, J.—Zhang, B.—Jia, W.—Wu, E.: Automatic Epicardial Fat Segmentation and Quantification of CT Scans Using Dual U-Nets with a Morphological Processing Layer. IEEE Access, Vol. 8, 2020, pp. 128032–128041, doi: 10.1109/ACCESS.2020.3008190.

[14] Godse, R.—Bhat, S.: Mathematical Morphology-Based Feature-Extraction Technique for Detection and Classification of Faults on Power Transmission Line. IEEE Access, Vol. 8, 2020, pp. 38459–38471, doi: 10.1109/ACCESS.2020.2975431.

[15] Challa, A.—Danda, S.—Sagar, B. S. D.—Najman, L.: Some Properties of Interpolations Using Mathematical Morphology. IEEE Transactions on Image Processing, Vol. 27, 2018, No. 4, pp. 2038–2048, doi: 10.1109/TIP.2018.2791566.

[16] Salazar-Colores, S.—Cabal-Yepez, E.—Ramos-Arreguin, J. M.—Botella, G.—Ledesma-Carrillo, L. M.—Ledesma, S.: A Fast Image Dehazing Algorithm Using Morphological Reconstruction. IEEE Transactions on Image Processing, Vol. 28, 2019, No. 5, pp. 2357–2366, doi: 10.1109/TIP.2018.2885490.

[17] Vichik, A.—Keshet, R.—Malah, D.: A General Framework for Tree-Based Morphology and Its Applications to Self-Dual Filtering. Image and Vision Computing, Vol. 28, 2010, No. 10, pp. 1443–1451, doi: 10.1016/j.imavis.2009.08.008.

[18] Zhao, H.—Liu, H.—Xu, J.—Deng, W.: Performance Prediction Using High-Order Differential Mathematical Morphology Gradient Spectrum Entropy and Extreme Learning Machine. IEEE Transactions on Instrumentation and Measurement, Vol. 69, 2020, No. 7, pp. 4165–4172, doi: 10.1109/TIM.2019.2948414.

[19] Heijmans, H. J. A. M.: Composing Morphological Filters. IEEE Transactions on Image Processing, Vol. 6, 1997, No. 5, pp. 713–723, doi: 10.1109/83.568928.

[20] Qidwai, U.—Chen, C. H.: Digital Image Processing: An Algorithmic Approach with MATLAB. 1st Edition. Chapman and Hall/CRC, 2009, doi: 10.1201/9781420079517.

[21] Sussner, P.: Lattice Fuzzy Transforms from the Perspective of Mathematical Morphology. Fuzzy Sets and Systems, Vol. 288, 2016, pp. 115–128, doi: 10.1016/j.fss.2015.09.018.

[22] Ronse, C.: Why Mathematical Morphology Needs Complete Lattices. Signal Processing, Vol. 21, 1990, No. 2, pp. 129–154, doi: 10.1016/0165-1684(90)90046-2.

[23] Haralick, R. M.—Sternberg, S. R.—Zhuang, X.: Image Analysis Using Mathematical Morphology. IEEE Transactions on Pattern Analysis and Machine Intelligence, Vol. PAMI-9, 1987, No. 4, pp. 532–550, doi: 10.1109/TPAMI.1987.4767941.

[24] Sun, Z.—Gao, X.—Zhang, D.: A Nonlocal Operator Model for Morphological Image Processing. 2017 IEEE International Conference on Image Processing (ICIP), 2017, pp. 230–234, doi: 10.1109/ICIP.2017.8296277.

[25] Soille, P.: Morphological Image Analysis: Principles and Applications. 2nd Edition. Springer, 2004, doi: 10.1007/978-3-662-05088-0.

[26] Maragos, P.—Vachier, C.: Overview of Adaptive Morphology: Trends and Perspectives. 2009 16th IEEE International Conference on Image Processing (ICIP), 2009, pp. 2241–2244, doi: 10.1109/ICIP.2009.5413961.

[27] Ćurić, V.—Landström, A.—Thurley, M. J.—Hendriks, C. L. L.: Adaptive Mathematical Morphology – A Survey of the Field. Pattern Recognition Letters, Vol. 47, 2014, pp. 18–28, doi: 10.1016/j.patrec.2014.02.022.

[28] Bobin, J.—Starck, J. L.—Fadili, J. M.—Moudden, Y.—Donoho, D. L.: Morphological Component Analysis: An Adaptive Thresholding Strategy. IEEE Transactions on Image Processing, Vol. 16, 2007, No. 11, pp. 2675–2681, doi: 10.1109/TIP.2007.907073.

[29] Roerdink, J. B. T. M.: Adaptivity and Group Invariance in Mathematical Morphology. 2009 16th IEEE International Conference on Image Processing (ICIP), 2009, pp. 2253–2256, doi: 10.1109/ICIP.2009.5413983.

[30] Lerallut, R.—Decencière, É.—Meyer, F.: Image Filtering Using Morphological Amoebas. Image and Vision Computing, Vol. 25, 2007, No. 4, pp. 395–404, doi: 10.1016/j.imavis.2006.04.018.

[31] Verd-Monedero, R.—Angulo, J.—Serra, J.: Anisotropic Morphological Filters with Spatially-Variant Structuring Elements Based on Image-Dependent Gradient Fields. IEEE Transactions on Image Processing, Vol. 20, 2011, No. 1, pp. 200–212, doi: 10.1109/TIP.2010.2056377.

[32] Bouaynaya, N.—Charif-Chefchaouni, M.—Schonfeld, D.: Spatially Variant Morphological Restoration and Skeleton Representation. IEEE Transactions on Image Processing, Vol. 15, 2006, No. 11, pp. 3579–3591, doi: 10.1109/TIP.2006.877475.

[33] Ta, V. T.—Elmoataz, A.—Lézoray, O.: Nonlocal PDEs-Based Morphology on Weighted Graphs for Image and Data Processing. IEEE Transactions on Image Processing, Vol. 20, 2011, No. 6, pp. 1504–1516, doi: 10.1109/TIP.2010.2101610.

[34] Cousty, J.—Najman, L.—Dias, F.—Serra, J.: Morphological Filtering on Graphs. Computer Vision and Image Understanding, Vol. 117, 2013, No. 4, pp. 370–385, doi: 10.1016/j.cviu.2012.08.016.

[35] Shih, H. C.—Liu, E. R.: Automatic Reference Color Selection for Adaptive Mathematical Morphology and Application in Image Segmentation. IEEE Transactions on Image Processing, Vol. 25, 2016, No. 10, pp. 4665–4676, doi: 10.1109/TIP.2016.2586658.

[36] Lei, T.—Jia, X.—Liu, T.—Liu, S.—Meng, H.—Nandi, A. K.: Adaptive Morphological Reconstruction for Seeded Image Segmentation. IEEE Transactions on Image Processing, Vol. 28, 2019, No. 11, pp. 5510–5523, doi: 10.1109/TIP.2019.2920514.

[37] Huang, W.—Liu, J.: Robust Seismic Image Interpolation with Mathematical Morphological Constraint. IEEE Transactions on Image Processing, Vol. 29, 2019, pp. 819–829, doi: 10.1109/TIP.2019.2936744.

[38] Milanfar, P.: A Tour of Modern Image Filtering: New Insights and Methods, Both Practical and Theoretical. IEEE Signal Processing Magazine, Vol. 30, 2013, No. 1, pp. 106–128, doi: 10.1109/MSP.2011.2179329.

[39] Treece, G.: The Bitonic Filter: Linear Filtering in an Edge-Preserving Morphological Framework. IEEE Transactions on Image Processing, Vol. 25, 2016, No. 11, pp. 5199–5211, doi: 10.1109/TIP.2016.2605302.

[40] Wang, J.—Guo, Y.—Ying, Y.—Liu, Y.—Peng, Q.: Fast Non-Local Algorithm for Image Denoising. 2006 International Conference on Image Processing, IEEE, 2006, pp. 1429–1432, doi: 10.1109/ICIP.2006.312698.

[41] He, K.—Sun, J.—Tang, X.: Guided Image Filtering. IEEE Transactions on Pattern Analysis and Machine Intelligence, Vol. 35, 2013, No. 6, pp. 1397–1409, doi: 10.1109/TPAMI.2012.213.

[42] Liu, C. W.—Kang, S. C.: A Video-Enabled Dynamic Site Planner. Computing in Civil and Building Engineering (2014), 2014, pp. 1562–1569, doi: 10.1061/9780784413616.194.

[43] Honda, N.—Ohsato, A.: Applications of Artificial Intelligence in Japan. Telematics and Informatics, Vol. 5, 1988, No. 1, pp. 39–52, doi: 10.1016/S0736-5853(88)80007-8.

[44] Hoppensteadt, F. C.: An Introduction to the Mathematics of Neurons: Modeling in the Frequency Domain. 2nd Edition. Cambridge University Press, 1997.

[45] Kuosmanen, P.—Astola, J.: Soft Morphological Filtering. Journal of Mathematical Imaging and Vision, Vol. 5, 1995, pp. 231–262, doi: 10.1007/BF01248374.

[46] Lei, T.—Jia, X.—Zhang, Y.—Liu, S.—Meng, H.—Nandi, A. K.: Superpixel-Based Fast Fuzzy C-Means Clustering for Color Image Segmentation. IEEE Transactions on Fuzzy Systems, Vol. 27, 2019, No. 9, pp. 1753–1766, doi: 10.1109/TFUZZ.2018.2889018.

[47] Wang, C.—Pedrycz, W.—Zhou, M. C.—Li, Z. W.: Sparse Regularization-Based Fuzzy C-Means Clustering Incorporating Morphological Grayscale Reconstruction and Wavelet Frames. IEEE Transactions on Fuzzy Systems, Vol. 29, 2021, No. 7, pp. 1826–1840, doi: 10.1109/TFUZZ.2020.2985930.

[48] Haralick, R. M.—Sternberg, S. R.—Zhuang, X.: Image Analysis Using Mathematical Morphology. IEEE Transactions on Pattern Analysis and Machine Intelligence, 1987, No. 4, pp. 532–550, doi: 10.1109/TPAMI.1987.4767941.

[49] Aptoula, E.—Lefèvre, S.: A Comparative Study on Multivariate Mathematical Morphology. Pattern Recognition, Vol. 40, 2007, No. 11, pp. 2914–2929, doi: 10.1016/j.patcog.2007.02.004.

[50] Wang, Z.—Bovik, A. C.—Sheikh, H. R.—Simoncelli, E. P.: Image Quality Assessment: From Error Visibility to Structural Similarity. IEEE Transactions on Image Processing, Vol. 13, 2004, No. 4, pp. 600–612, doi: 10.1109/TIP.2003.819861.

[51] Mellouli, D.—Hamdani, T. M.—Sanchez-Medina, J. J.—Ayed, M. B.—Alimi, A. M.: Morphological Convolutional Neural Network Architecture for Digit Recognition. IEEE Transactions on Neural Networks and Learning Systems, Vol. 30, 2019, No. 9, pp. 2876–2885, doi: 10.1109/TNNLS.2018.2890334.

[52] Roy, S. K.—Mondal, R.—Paoletti, M. E.—Haut, J. M.—Plaza, A.: Morphological Convolutional Neural Networks for Hyperspectral Image Classification. IEEE Journal of Selected Topics in Applied Earth Observations and Remote Sensing, Vol. 14, 2021, pp. 8689–8702, doi: 10.1109/JSTARS.2021.3088228.

[53] Fujisaki, H.—Nakashizuka, M.: Deep Morphological Filter Networks for Gaussian Denoising. 2020 IEEE International Conference on Image Processing (ICIP), 2020, pp. 918–922, doi: 10.1109/ICIP40778.2020.9190657.

Mingzhu Zhang received her B.Sc. degree in mathematics from the Linyi University, Linyi, China, in 2020, and her M.Sc. degree in mathematics from the Liaocheng University, Liaocheng, China, in 2024. Currently, she is pursuing the Ph.D. degree from the Chongqing University of Posts and Telecommunications, Chongqing, China. Her research interests include image processing and machine learning.

Mengdi Sun received her B.Sc. degree in mathematics from the Binzhou University, Binzhou, China, in 2019, and her M.Sc. degree in mathematics from the Liaocheng University, Liaocheng, China, in 2022. Currently, she is a teacher at the Dong'e Nanhu Xingzhi School, Dong'e, China.

Huichao Sun received his B.Sc. degree in mathematics from the Dezhou University, Dezhou, China, in 2021, and his M.Sc. degree in mathematics from the Liaocheng University, Liaocheng, China, in 2024. Currently, he is pursuing the Ph.D. degree from the Shandong Normal University, Jinan, China. His research interests include image processing and machine learning.

Zhonggui Sun received his B.Sc. degree in mathematics from the Shandong Normal University, China, in 1996. In 2006, he received his M.Sc. degree in computer software and theory from the Sichuan Normal University, China. And in 2014, he received his Ph.D. degree in computer application technology from the Nanjing University of Aeronautics and Astronautics, China. From 2016 to 2017, he was a visiting scholar at the Xidian University, China. Currently, he is Professor at the School of Mathematical Sciences, Liaocheng University, China. His research interests include image processing and machine learning.